Research Square

Preprints are preliminary reports that have not undergone peer review.
They should not be considered conclusive, used to inform clinical practice,
or referenced by the media as validated information.

SIRT2 promotes spinal cord injury repair by inhibiting ferroptosis through the regulation of the p53/Nrf2 pathway

Zijing Zhang
Affiliated Zhongshan Hospital of Dalian University
Shengbo Shi
Affiliated Zhongshan Hospital of Dalian University
Yanfang Hou
Department of Rehabilitation Medicine, Shangqiu Suiyang District Traditional Chinese Medicine Hospital
Cunheng Yang
Xuan Wu Hospital of the Capital Medical University
Hua Zhai
Capital Medical University
Wangwei Zhu
Affiliated Zhongshan Hospital of Dalian University
Zetian Zhao
Affiliated Zhongshan Hospital of Dalian University
Zhe Wang
Affiliated Zhongshan Hospital of Dalian University
Tienan Wang
Affiliated Zhongshan Hospital of Dalian University
Yu Zhou
Affiliated Zhongshan Hospital of Dalian University
Meng Zhang
Affiliated Zhongshan Hospital of Dalian University
Junxiao Gao
Affiliated Zhongshan Hospital of Dalian University
Lu Qin
Affiliated Zhongshan Hospital of Dalian University
Xiaobing Yu
yuxiaobing1976@hotmail.com

Affiliated Zhongshan Hospital of Dalian University

Research Article

Keywords: Spinal cord injury, Sirtuin2, p53/Nrf2 signaling pathway, oxidative stress, ferroptosis, Neural injury and repair, functional recovery, neuron

Posted Date: July 20th, 2026

DOI: https://doi.org/10.21203/rs.3.rs-10379046/v1

License: This work is licensed under a Creative Commons Attribution 4.0 International License.
Read Full License

Additional Declarations: No competing interests reported.

Abstract

Spinal cord injury (SCI) is a severe traumatic disease of the central nervous system, typically leading to partial or complete loss of sensory and motor functions.The lipid peroxidation apoptosis process caused by iron overload is known as ferroptosis. As a novel form of programmed cell death, ferroptosis has become a research focus in the study of cell death mechanisms following SCI.This study aims to explore the role and potential mechanisms of Silent Information Regulator 2 (SIRT2) in inhibiting ferroptosis and promoting injury repair after SCI by regulating the p53/Nrf2 pathway.By constructing cell models and rat SCI models, we analyzed the expression changes of SIRT2, p53, Nrf2, as well as iron ions, oxidative stress markers, and ferroptosis-related markers (such as GPX4 and 4HNE).Experimental results showed that after SCI, the expression of SIRT2 significantly decreased, while the activation of p53 and inhibition of Nrf2 exacerbated iron overload and lipid peroxidation, leading to ferroptosis and worsening cell damage.By transfecting PC12 cells with recombinant adenovirus overexpressing SIRT2, we found that SIRT2 can reduce ferroptosis by inhibiting p53 activity and activating the Nrf2 pathway, thereby alleviating cell damage.Further, after intrathecal injection of recombinant adenovirus overexpressing SIRT2, we found a certain degree of recovery in central nervous cells and motor function in rats.Additionally, using the specific p53 activator (Nutlin-3a), we further validated the regulatory effect of SIRT2 on the p53/Nrf2 pathway.This study reveals a new mechanism by which SIRT2 inhibits ferroptosis through the regulation of the p53/Nrf2 pathway, providing new strategies for the treatment of SCI.

1 Introduction

Spinal cord injury (SCI) is a common traumatic disease of the central nervous system caused by external injury, imposing severe psychological stress and economic burden on patients and their families (1). SCI is divided into primary and secondary injury phases. Especially in the acute phase, SCI triggers a series of physiological and pathological processes, including free radical production, oxidative damage, inflammatory responses, and vascular injury (2). Early intervention in the injury phase can effectively mitigate further deterioration. Despite recent advances in SCI treatment and rehabilitation, many challenges remain (3). Recent studies have shown that SCI is closely associated with ferroptosis (4). As a novel form of programmed cell death, ferroptosis is characterized by alterations in iron metabolism, iron-induced reactive oxygen species (ROS) accumulation, inhibition of glutathione peroxidase 4 (GPX4), and increased lipid peroxidation (5). Unlike apoptosis and autophagy, ferroptosis is induced by the accumulation of iron ions, leading to elevated lipid peroxides and consequent cell damage and death (6). Meanwhile, ongoing cell death exacerbates the severity of SCI (7). Studies have shown that ferritin is highly expressed in SCI and positively correlates with its severity (7). Therefore, interventions targeting ferroptosis may become an effective new strategy for treating SCI (8). By inhibiting the ferroptosis pathway, we may improve neurological function post-SCI, providing new directions and targets for clinical treatment (9).

Sirtuins (SIRTs) are part of the Silent Information Regulator protein family, a class of NAD+-dependent protein deacetylases that play crucial roles in cellular signal transduction and various biological processes (10). SIRT2, a member of the Sirtuins protein family, has broad functions, including the regulation of mitosis, cell cycle, and metabolic pathways (11). In the context of neurodegenerative diseases, SIRT2 has gained attention for its role in regulating the aggregation of α-synuclein associated with Parkinson's disease (12). Additionally, studies suggest that SIRT2 may regulate lipid metabolism and insulin sensitivity, highlighting its potential as a therapeutic target for metabolic diseases (13). More importantly, the role of SIRT2 in inhibiting ferroptosis and promoting SCI repair underscores its significance in cellular stress response and neuroprotection (14). p53 is a tumor suppressor protein widely involved in cell cycle regulation, DNA repair, apoptosis, and oxidative stress responses (15). It can also influence the expression of iron metabolism-related genes, such as ferritin and iron transport proteins, thus affecting intracellular iron concentrations (16). Through this regulation, p53 may indirectly affect the occurrence of ferroptosis. Previous studies have shown that SIRT2 can directly deacetylate p53, affecting its activity and stability (17). Deacetylation generally weakens p53’s transcriptional activity, reducing its ability to promote cell cycle arrest and apoptosis. SIRT2 may indirectly promote Nrf2-dependent gene expression by deacetylating certain transcription factors or core repressor proteins(18). Under oxidative stress conditions, the expression and activity of SIRT2 may change, thereby affecting Nrf2 regulatory mechanisms. The activation of SIRT2 helps maintain cellular energy balance and enhances its antioxidant defense, potentially mediated indirectly through the Nrf2 pathway (19). Nrf2 activation provides cellular protection by promoting the expression of glutathione peroxidase 4 (GPX4), preventing lipid peroxidation and cell damage caused by iron overload (20). However, the precise molecular mechanisms of their roles in SCI remain unclear.

Unraveling these mechanisms may reveal new therapeutic targets for SCI. Based on the above research background, we hypothesize that SIRT2 regulates ferroptosis-induced SCI by inhibiting p53 and upregulating Nrf2. Overexpressing SIRT2 may suppress ferroptosis-induced SCI and partially restore motor function in SCI rats. To test this hypothesis, we established in vitro and in vivo SCI models and investigated the regulation of SIRT2 and its effects on the p53/Nrf2 pathway and ferroptosis in SCI, elucidating its potential molecular mechanisms.

2 Materials and Methods

2.1 Cell Collection

PC12 cells belong to the adrenal pheochromocytoma cell line, derived from neural cells, and have physiological characteristics similar to neurons, commonly used in central nervous system-related research.Rat pheochromocytoma cells (PC12) were purchased from the Chinese Academy of Sciences Cell Bank (Shanghai, China) and cultured in Dulbecco's Modified Eagle Medium (DMEM) containing 10% horse serum and 5% fetal bovine serum.The cells were cultured in a humidified incubator at 37°C with 95% air and 5% CO2.In in vitro drug treatment experiments, RAS-selective-lethal-3 (Rsl3, CSN17581, CSNpharm) is a classic ferroptosis inducer. 5 μM Rsl3 can induce ferroptosis in PC12 cells.

2.2 Evaluation of the Therapeutic Efficacy of SIRT2 Overexpression Recombinant Adenovirus

The efficacy was validated using PC12 cells. Wild-type cells were used as a negative control, and cells transfected with negative control adenovirus served as a pure virus control. The experimental group was transfected with adenovirus overexpressing SIRT2.Transfection was performed using a semi-infection method when cells reached 50% confluence. Specifically, after removing half of the culture medium, fresh medium containing adenovirus was added. After 4 hours, the medium was restored to its original volume, and 6 hours later, the medium was completely replaced with fresh medium.After 48 hours of transfection, fluorescence intensity was detected using a fluorescence microscope, and target gene expression was quantified using qRT-PCR to evaluate transfection efficiency.

2.3 Cell Counting Kit-8 (CCK-8) Assay

According to the manufacturer's instructions, cell viability was assessed using the Cell Counting Kit-8 (CCK-8, LJ621, Dojindo, Japan).Cells were seeded in 96-well flat-bottom microtiter plates at a density of 1.5×10^4 cells per well. After 24 hours, Rsl3 was added at specified concentrations at different time points (6, 12, 24, and 48 hours).Absorbance at 450 nm was measured using a microplate reader (Synergy HT, Bio-Tek, USA).

2.4 Measurement of ROS, SOD, MPO and 4HNE

According to the manufacturer's instructions, the activities of reactive oxygen species (ROS), superoxide dismutase (SOD), myeloperoxidase (MPO), and 4-hydroxymonoene (4HNE) in PC12 cells were determined using the corresponding kits from Solarbio (Beijing, China). Operate in accordance with the kit instructions. The level of 4-hydroxynonenal (Cat#YPJ1152, UpingBio) was determined by enzyme-linked immunosorbent assay (ELISA).

2.5 Measurement of Iron, Glutathione, and Malondialdehyde

First, collect the samples. To determine the iron concentration, use the tissue iron detection kit (A039-2-1, Nanjing Jiancheng Bioengineering Institute, Nanjing, China). According to the manufacturer's instructions, use a spectrophotometer (Varioskan Flash; Thermo Scientific) to measure and read the optical density (OD) value at 520 nm. Then, determine the iron concentration in all samples by comparing the OD of the sample with the standard curve. The reduced glutathione (GSH) content detection kit (BC1170, Solarbio, Beijing, China) uses visible spectrophotometry to determine the GSH content in the samples. Operate according to the kit instructions and calculate the GSH content in each group of samples. The malondialdehyde (MDA) content determination kit (A003-101, Nanjing Jiancheng Bioengineering Institute, Nanjing, China) uses the thiobarbituric acid (TBA) reaction method to determine the malondialdehyde (MDA) content in the samples. Operate according to the kit instructions and calculate the MDA content of each group of samples.

2.6 Experimental Animal Preparation

Due to physiological and hormonal differences, especially the influence of estrogen, iron metabolism differs between female and male rats. Therefore, male rats were used to study ferroptosis.In SCI patients, the male-to-female ratio is approximately 4:1, making male rats more suitable for SCI research.Forty adult male Sprague-Dawley rats (8–10 weeks old, 230–250 g) were used in the experiments. They were housed under controlled conditions of light cycle (12-hour light/dark), temperature (22–25°C), and humidity (55–60%), with three rats per cage, and allowed free access to food and water.All experimental procedures were conducted under the supervision of the Ethics Committee of Zhongshan Hospital, Dalian University (Approval No. DWS2024-063-01), and in accordance with the NIH Guide for the Care and Use of Laboratory Animals.

2.7 Establishment of SCI Rat Model

SCI was induced using a T9-T10 spinal cord hemisection. Forty rats were randomly divided into four groups: Sham group, SCI group, SCI + adenovirus control vector group (SCI + Ad-control group), and SCI + adenovirus SIRT2 vector group (SCI + Ad-SIRT2 group). After one week of acclimation, the rats were anesthetized with 3% isoflurane (R510-22-10, RWD Life Science, Shenzhen, China) for induction and maintained with 2% isoflurane (2–3 L/min). A midline skin incision was made on the back, and the muscles were separated to expose the spinal processes and the lamina of the thoracic (T10) segment. A precise impactor device (68099II, RWD Life Science) was used to induce SCI with parameters set to a speed of 2 m/s, a depth of 1 mm, and a dwell time of 0.4 seconds, causing moderate contusion (60 kdyn). Immediately after modeling, spinal cord bleeding and swelling were observed. Successful establishment of the SCI model was indicated by involuntary spasms in the hind limbs and tail twisting. After recovery from anesthesia, muscle strength loss and paralysis were also noted. The Sham group underwent the same surgical procedures except for the spinal cord contusion. During surgery, the body temperature was maintained at 37 ± 0.3°C using a heating pad. Post-surgery, successful SCI modeling was indicated by flaccid paralysis of the hind limbs and tail. After modeling, all rats were manually voided twice daily until bladder function was restored. Surgeries were performed under anesthesia with minimal pain. All animal experimental protocols adhered to Chinese animal welfare legislation for the care and use of animals.

2.8 Construction of Recombinant Adenovirus

The target gene sequence obtained from the NCBI Gene Bank was cloned into the pAdTrack-CMV-3flag vector to construct the target gene plasmid. This plasmid was then recombined with the adenoviral backbone plasmid pAdeasy-1 to generate the final overexpression recombinant adenovirus. Hanbio Biotechnology Co., Ltd. (Shanghai, China) constructed the empty control adenovirus and the SIRT1 overexpression adenovirus and performed sequencing.

2.9 Animal Treatment

The target gene sequence obtained from the NCBI Gene Bank was cloned into the pAdTrack-CMV-3flag vector to construct the target gene plasmid. This plasmid was then recombined with the adenoviral backbone plasmid pAdeasy-1 to generate the final overexpression recombinant adenovirus. Hanbio Biotechnology Co., Ltd. (Shanghai, China) constructed the empty control adenovirus and the SIRT1 overexpression adenovirus and performed sequencing.

2.10 Adenovirus Injection

Recombinant adenovirus overexpressing SIRT2 (Ad-SIRT2) was purchased from Hanbio Biotechnology Co., Ltd. (Shanghai, China). The SCI + Ad-control and SCI + Ad-SIRT2 groups received adenovirus-mediated injections twice weekly for five weeks, starting on the first day post-SCI. The adenovirus dose was 1 × 10^8 pfu/mL. Rats were anesthetized with 3% isoflurane and maintained with 2% isoflurane. The rats were placed in a prone position on the operating table, and a microsyringe was used to inject the adenovirus vertically 0.5 cm anterior to the injury site. The Sham and SCI groups were injected with an equal volume of saline. After five weeks, the rats were anesthetized, euthanized by cervical dislocation, and spinal cord tissue and serum were collected.

2.11 Basso-Beattie-Bresnahan (BBB) Locomotor Rating Scale

The Basso, Beattie, and Bresnahan (BBB) locomotor rating scale is a commonly used tool for assessing behavioral outcomes after SCI in rats. Scores range from 0 to 21, where 0 indicates no motor function and 21 indicates normal motor function. Rats were allowed to walk freely for 5 minutes, and hind limb movements were closely observed. On days 1, 3, 7, 14, 21, and 28 post-surgery, two independent examiners evaluated the locomotor recovery of all groups using the BBB scale.

2.12 Rivlin Inclined Plane Test

The inclined plane test was conducted using the Rivlin method. An adjustable-tilt apparatus was employed, on which a piece of cardboard was placed and covered with a 6-mm thick rubber pad. The rat was positioned on the rubber pad along its body length. The inclination angle was gradually increased until the rat could stably stand on the inclined plane for 5 seconds. At this point, the angle of the inclined plane was measured. Each rat was measured three times, and the average value was recorded.

2.13 Tissue Sampling and Section Preparation

Five weeks post-SCI surgery, the entire spinal cord was dissected and its anterior-posterior orientation was marked. A 3-cm segment of spinal cord tissue was taken from the injury center and immersed in PBS containing 4% paraformaldehyde, stored at 4°C for one week. The paraffin-embedded samples were then sectioned into 5-μm slices and evaluated for pathological changes using hematoxylin-eosin (HE) and Nissl staining.

2.14 Hematoxylin-Eosin Staining

The sections were successively immersed in xylene, absolute ethanol, and ethanol for deparaffinization, followed by a rinse with tap water. The sections were stained with hematoxylin for 3–5 minutes, rinsed with tap water, differentiated, and washed with tap water again. The sections were then restored to blue color using a blueing buffer. After rinsing with running water, the sections were dehydrated in 85% and 95% ethanol for 5 minutes each and stained with eosin for 5 minutes. Subsequently, the sections were dehydrated in ethanol of increasing concentrations for 5 minutes each, cleared in xylene for 5 minutes, and mounted with neutral gum. Under the light microscope, the nuclei appeared blue, the cytoplasm red, and collagen and muscle fibers light pink.

2.15 Nissl Staining

After routine deparaffinization, the sections were stained with methylene blue for 10 minutes and differentiated with Nissl for 1–3 minutes until Nissl bodies were clearly visible under the microscope. The sections were then treated with ammonium molybdate solution for 3–5 minutes, followed by a quick rinse with distilled water to prevent discoloration. They were then dehydrated with absolute ethanol, cleared with xylene, and mounted with neutral gum. Finally, neuronal images were analyzed under an optical microscope using image processing software (Media Cybernetics, Silver Springs, MD, USA).

2.16 Quantitative Reverse Transcription Polymerase Chain Reaction (qRT-PCR)

Tissue samples from the injury site and approximately 5 mm surrounding it were collected. Total RNA was extracted from cells and spinal cord tissue using the StradyPure Universal RNA Extraction Kit (StradyPure, China). Reverse transcription was performed using the PrimeScript™ RT Reagent Kit (TaKaRa, Tokyo, Japan) or the miRCURY LNA Universal cDNA Synthesis Kit (Exiqon, Vedbaek, Denmark), following the manufacturers' protocols. Gene expression levels were detected using a LightCycler 480 qRT-PCR System (Roche Diagnostics, Indianapolis, IN, USA) according to the SYBR Green Mix qRT-PCR Kit (Roche Diagnostics) instructions. The thermal cycling parameters were as follows: 95°C for 5 minutes for initial denaturation, followed by 40 cycles of 95°C for 5 seconds, 60°C for 10 seconds, and 72°C for 10 seconds, with a final extension at 72°C for 5 minutes. Each qRT-PCR reaction was performed in triplicate. Data were analyzed using the 2-ΔΔCt method, with glyceraldehyde-3-phosphate dehydrogenase (GAPDH) or U6 as the internal control: ΔΔCt = (Ct_target gene - Ct_internal control)_experiment - (Ct_target gene - Ct_internal control)_control. The relevant primers were synthesized by Sangon (Shanghai, China) (Table 1).

Table 1
Primer sequences for qRT-PCR

Gene name	Primer sequences
SIRT2	F: 5'-ATGGCGACCTGGCTTCTG-3'
	R: 5'-TCAGTGCTGCTGTCCTTCC-3'
Nrf2	F: 5'-GCTGCCATTAGTCAGTCGCTCTC-3'
	R: 5'-ACCGTGCCTTCAGTGTGCTTC-3'
P53	F: 5'-ATGACTGAGGTCGTGAGACG-3'
	R: 5'-GCATACGGATTTCCTTCCAC-3'
GPX4	F: 5'-ATGGCTGCCCAAGGCTTAC-3'
	R: 5'-TTAGCCATCGGTCAGCATCC-3'

2.17Western blot analysis

Tissue samples from the injury site and approximately 5 mm surrounding it were collected. The tissues were homogenized in RIPA lysis buffer (Zhongshan Golden Bridge, China) containing protease inhibitors (Sigma, China). For cell samples, cells were digested with trypsin following standard procedures, centrifuged at 1000 rpm for 5 minutes, transferred to 1.5 mL centrifuge tubes, and washed three times with PBS. Lysis buffer was added at a ratio of 100 μL RIPA + 1 μL PMSF (100 mM). The cells were resuspended and incubated on ice for 30 minutes. The lysate was then centrifuged at 12000 rpm for 30 minutes at 4°C, and the supernatant was collected.

Protein concentrations were determined using the BCA assay. BCA working reagent was prepared according to the specified ratio. Standards were diluted and added to a 96-well plate along with equal volumes of samples. The absorbance at 450 nm was measured with a microplate reader, and protein concentrations were calculated based on a standard curve. SDS-PAGE was performed, followed by gel electrophoresis at a specified voltage until proteins reached an appropriate position. Proteins were then transferred onto a PVDF membrane. After pre-treating the membrane, a transfer stack was formed and placed in a transfer clamp. The proteins were transferred at a specific current under low temperature conditions based on molecular weight.

For immunoblotting, the membrane was washed and blocked before incubating with primary antibodies overnight at 4°C. After multiple washes, the membrane was incubated with secondary antibodies. The membrane was then placed on a transparent plastic plate, and chemiluminescent substrate was evenly added. Chemiluminescence was performed, and protein bands were quantitatively analyzed using Image J software (NIH, Bethesda, MD, USA), with GAPDH as the internal control. Each experiment was repeated three times.

The following primary antibodies were used at specified dilutions: SIRT2 Polyclonal antibody (19655-1-AP, Proteintech, USA, 1:5000), p53 Monoclonal antibody (60283-2-Ig, Proteintech, USA, 1:1000), Nrf2, NFE2L2 Recombinant antibody (80593-1-RR, Proteintech, USA, 1:1000), GPX4 Monoclonal antibody (67763-1-Ig, Proteintech, USA, 1:1000), Anti-4 Hydroxynonenal antibody [HNEJ-2] (Abcam, UK, 1:1000), GAPDH (ab8245, Abcam, UK, 1:2000), Goat Anti-Mouse IgG/HRP (SE131, Solarbio, China, 1:2000), Goat Anti-Rabbit IgG H&L (HRP) (ab6721, Abcam, UK, 1:2000).

2.18 Immunofluorescence assessment

The spinal cord tissue was fixed with 4% paraformaldehyde solution (BL 539 A, Biosharp). Subsequently, the spinal cord tissue was dehydrated by graded sucrose solutions (15% and 30%, respectively). After dehydration, the spinal cord tissue was embedded and then sectioned into 10 μm frozen axial sections using a cryostat (CM 1950, Leica). The frozen sections (10 μm) were thawed at room temperature and re-fixed with 4% paraformaldehyde for 30 minutes. Next, 0.3% Triton X-100 (Triton (Beijing Zhongshan Jinqiao, Triton X-100)) was added for 15 minutes, followed by incubation with 10% normal goat serum (AR 0009, Boster, Wuhan, China) at room temperature for 1 hour. Then, primary antibodies were added and the sections were incubated overnight at 4°C in a humid chamber. The sections were rinsed three times in PBS containing Tween (PBST), and then incubated with fluorescein isothiocyanate and secondary antibodies at room temperature for 1 hour. Thereafter, the sections were rinsed three times with PBST and stained with 4',6-diamidino-2-phenylindole (DAPI) (Shanghai Beyotime, P0103) for 15 seconds. The expression of target proteins in spinal cord tissue was observed by the Mingmei microscopic digital imaging system (Mingmei). Images were analyzed using ImageJ software (v1.8.0). The antibodies employed were: Rabbit Anti-Mouse IgG H&L (HRP) (ab6728, abcam), Goat Anti-Rabbit IgG H&L (HRP) (ab6721, abcam), SIRT2 (19655-1-AP, proteintech, 1:200), P53 (10442-1-AP, proteintech, 1:200), Nrf2 (16396-1-AP, proteintech, 1:200), GPX4 (67763-1-Ig, proteintech, 1:200), and 4HNE (ab48506, abcam, 1:200).

2.19 Transmission electron microscopy

The sample preparation protocol for transmission electron microscopy (TEM) proceeds as follows: Fresh tissue specimens are promptly dissected within 1–3 minutes post-excision into 1 mm^3 fragments under pre-cooled TEM fixative protection, followed by immediate immersion in fresh fixative for 4°C storage. After three sequential rinses (15 minutes each) with 0.1 M phosphate buffer (PB, pH 7.4), secondary fixation is performed using 1% osmium tetroxide in 0.1 M PB under light-protected conditions at room temperature for 2 hours, succeeded by additional buffer rinses. Dehydration is achieved through a graded ethanol series (30%, 50%, 70%, 80%, 95%, 100%, 20 minutes per concentration) and two 15-minute acetone treatments. Stepwise infiltration with 812 epoxy resin(90529-77-4,SPI) is conducted sequentially: acetone-resin mixtures (1:1 for 2–4 hours; 1:2 overnight at 37°C), followed by pure resin infiltration for 5–8 hours before mold embedding at 37°C. Polymerization is executed in a 60°C oven for 48 hours. Ultrathin sections (60–80 nm) are prepared using an ultramicrotome(Leica UC7, Leica)and mounted on 150-mesh copper grids. Dual electron staining involves 8-minute treatments with 2% uranyl acetate in ethanol (light-protected) and 2.6% lead citrate (CO_2-free environment), each followed by three

ultrapure water rinses. After air-drying overnight at ambient temperature, specimens are subjected to TEM(Tecnai F20, FEI, Hillsboro, Oregon, USA). imaging and structural analysis. Strict adherence to temporal, thermal, and concentration parameters throughout this protocol is critical for maintaining ultrastructural preservation.

2.20 Statistical Analysis

All analyses were conducted by researchers blinded to the experimental conditions. Data processing, statistical analysis, and graph generation were performed using GraphPad Prism 9.0 software (GraphPad Software, San Diego, CA, USA, www.graphpad.com). Two-way ANOVA and Tukey's post-hoc test were used for analyzing BBB scores and inclined plane test data. Other data were analyzed using one-way ANOVA followed by Dunnett's post-hoc test. A p-value of < 0.05 was considered statistically significant.

3 Results

3.1 Overexpression of SIRT2 Inhibits Oxidative Stress in PC12 Cells

To verify the regulatory role of SIRT2 in PC12 cells, we divided the cells into five groups: the sham group, SCI group, SCI + Ad-control group, SCI + Ad-SIRT2 group, and SCI + Ad-SIRT2 + Nutlin-3a group. Ferroptosis in PC12 cells was induced with 5 μM Rsl3 to simulate neuronal cell ferroptosis post-SCI. Nutlin-3a enhances p53 expression; thus, adding Nutlin-3a to the SCI + Ad-SIRT2 group allowed further verification of p53's impact on SCI.

To assess the efficiency of SIRT2 overexpression, PC12 cells were transfected with wild-type adenovirus (control), overexpression control adenovirus, or SIRT2 overexpression adenovirus. Successful transfection was confirmed by fluorescence microscopy, with the expression of enhanced green fluorescent protein (EGFP) indicating transfection success in the control and SIRT2 overexpression groups (Fig. 1A). Additionally, qRT-PCR analysis showed a significant increase in SIRT2 expression in the SIRT2 overexpression cells compared to the control group (Fig. 1B) ($P < 0.05$).

ELISA results indicated that, compared to the sham group, the SCI group had significantly elevated levels of ROS and MPO and significantly decreased levels of SOD. The SCI + Ad-control group exhibited similar changes to the SCI group, while the SCI + Ad-SIRT2 group showed the opposite trend. In the SCI + Ad-SIRT2 + Nutlin-3a group, the changes in these markers resembled those in the SCI and SCI + Ad-control groups (Fig. 1C). This suggests that SIRT2 overexpression can inhibit oxidative stress following ferroptosis in PC12 cells, and the regulatory process may involve p53, as inferred from the SCI + Ad-SIRT2 + Nutlin-3a group.

(A):The fluorescence images of transfected PC12 cells in the SIRT1 intervention group and the blank vector control group, Scale bar : 50 μm.(B):qRT-PCR analysis of SIRT2 expression levels

(C):Measurement of intracellular ROS, MPO, and SOD levels.(*P < 0.05, **P<0.01, ***P<0.001, ****P<0.0001 vs.SCI group;***P<0.001 vs.0 μmol/L group)

3.2 SIRT2 Inhibits Ferroptosis in PC12 Cells by Regulating p53 and Nrf2

Based on the above findings, SIRT2 may influence oxidative stress post-SCI through p53. Given that oxidative stress often precedes ferroptosis, we hypothesized that SIRT2 could also inhibit ferroptosis in PC12 cells, potentially involving p53 and other genes. We used qRT-PCR to assess the expression of SIRT2, p53, Nrf2, and ferroptosis markers GPX4 in cells transfected with adenoviruses, and the content of 4HNE.

The results showed that, compared to the sham group, SIRT2 expression was significantly reduced in the SCI group, indicating that ferroptosis induction downregulates SIRT2 expression in PC12 cells. The SCI + Ad-control group exhibited similar SIRT2 levels to the SCI group. Both groups showed increased p53 and decreased Nrf2 levels. Additionally, ferroptosis-related gene GPX4 levels were reduced, while ferroptosis-related markers 4HNE levels were elevated, suggesting that SIRT2, Nrf2, and p53 are involved in ferroptosis in PC12 cells.

In the SCI + Ad-SIRT2 group, SIRT2 levels were significantly higher compared to the sham, SCI, and SCI + Ad-control groups. This group also exhibited reduced p53 and increased Nrf2 levels. Ferroptosis-related gene GPX4 levels were higher, and ferroptosis-related markers 4HNE levels were lower compared to the previous groups. This indicates that overexpressing SIRT2 may inhibit p53 expression, thereby promoting Nrf2 expression and ultimately alleviating ferroptosis in PC12 cells. The SCI + Ad-SIRT2 + Nutlin-3a group further supported this idea. Adding a p53 agonist to cells overexpressing SIRT2 resulted in significantly elevated p53 levels and reduced Nrf2 and GPX4 levels compared to the SCI + Ad-SIRT2 group, similar to those in the SCI and SCI + Ad-control groups. This supports the hypothesis that SIRT2 inhibits ferroptosis in PC12 cells by regulating p53 and Nrf2(Fig. 2A,B) .

We further explored the interactions between these pathways through Western Blot (WB) experiments. The results showed that in the SCI and SCI + Ad-control groups, SIRT2 and Nrf2 levels were significantly lower, while p53 levels were significantly higher compared to the sham group. Ferroptosis-related protein GPX4 was significantly reduced, and ferroptosis-related markers 4HNE levels were elevated in these groups. Overexpression of SIRT2 reversed these protein expression levels(Fig. 2C). These findings confirm that SIRT2 overexpression promotes Nrf2 expression by downregulating p53, thereby inhibiting ferroptosis in PC12 cells.

A: mRNA expression levels of SIRT2, p53, and Nrf2.B: mRNA expression levels of GPX4 and measurement of intracellular 4HNE level.C: Western blot bands for SIRT2, p53, Nrf2, GPX4, 4HNE, and GAPDH. (*P < 0.05, **P < 0.01, ***P < 0.001, ****P < 0.0001 vs. SCI group)

3.3 Overexpression of SIRT2 Adenovirus Inhibits Ferroptosis Post-SCI in Rats

To better understand the mechanism by which SIRT2 regulates SCI, we divided 40 SCI rats into four groups: sham group, SCI group, SCI + Ad-control group, and SCI + Ad-SIRT2 group. In the SCI + Ad-SIRT2 group, we upregulated SIRT2 expression in the spinal cord through intrathecal injection of Ad-SIRT2, while the SCI + Ad-control group received intrathecal injections of Ad-control for comparison.

Results showed that in the spinal cord tissue at the injury site, GSH levels were significantly lower, and MDA and iron levels were significantly higher in the SCI group compared to the sham group. The SCI + Ad-control group showed similar changes to the SCI group, whereas the SCI + Ad-SIRT2 group exhibited opposite trends in these factors(Fig. 3A). This indicates that spinal cord neurons may undergo ferroptosis after SCI, and overexpression of SIRT2 may inhibit this process through certain pathways.

Further qRT-PCR and Elisa analysis revealed that SIRT2 overexpression can regulate the expression of ferroptosis-related genes by inhibiting p53 and upregulating Nrf2, thereby preventing ferroptosis(Fig. 3B,C). This finding is consistent with our previous cellular experiments. Western Blot (WB) analysis confirmed the expression of pathway proteins and ferroptosis-related proteins among the four groups(Fig. 3D). We observed differences in the expression of SIRT2, P53, Nrf2, GPX4 and 4HNE in spinal cord tissue through immunofluorescence staining of spinal cord tissue sections from each group (Fig. 3E), which are similar to the above experimental results. The results showed that SIRT2 and Nrf2 expressions were significantly reduced in the spinal cord tissue of SCI rats compared to the sham group, while p53 expression was significantly increased. Overexpression of SIRT2 inhibited the expression of p53 and increased the expression of Nrf2 in SCI rats' spinal cord tissue, thereby regulating the expression of ferroptosis-related proteins and inhibiting ferroptosis.Transmission electron microscopy revealed pathological alterations in the mitochondrial structure of spinal cord neurons in both the SCI group and the SCI + Ad-control group. These changes encompassed mitochondrial shrinkage and reduction or disappearance of cristae. The SCI + Ad-SIRT2 group mitigated these pathological changes. The structure and morphology of mitochondria were improved in the SCI + Ad-SIRT2 group (Fig. 3F).

Our animal experiments further confirmed that SIRT2 can inhibit ferroptosis in SCI rats by regulating the p53/Nrf2 pathway.

A: Measurement of iron, GSH, and MDA levels in spinal cord tissues of each group.B: mRNA expression levels of SIRT2, p53, and Nrf2 in spinal cord tissues of each group.C: mRNA expression levels of GPX4 and measurement of 4HNE level in spinal cord tissues of each group.D: Western blot bands for SIRT2, p53, Nrf2, GPX4, 4HNE, and GAPDH in spinal cord tissues of each group (N = 10; *P < 0.05, **P < 0.01, ***P < 0.001, ****P < 0.0001). E: Immunofluorescence study on the expression of SIRT2, P53, Nrf2, GPX4 and 4HNE in spinal cord tissue of rats with spinal cord injury. Fluorescence microscopy results of SIRT2, P53, Nrf2, GPX4 and 4HNE and DAPI. Green indicates SIRT2, P53, Nrf2, GPX4 and 4HNE in spinal cord tissue, and blue indicates nuclei stained by DAPI. Scale bar: 50 μm. F:Transmission electron microscopy

images. The morphology of mitochondria differs between groups. Arrows show mitochondria of spinal cord neurons. Boxes show high magnification views of low magnification images. Scale bars: 1 μm (upper panels) and 500 nm (lower panels).

3.4 SIRT2 Inhibits Neuronal Damage and Promotes Motor Function Recovery in SCI Rats Through the p53/Nrf2 Pathway

To further validate the above hypotheses, we used hematoxylin-eosin (HE) staining and Nissl staining to observe and assess the structural changes and neuronal recovery at the lesion site post-SCI. The results showed that, compared to the sham group, the SCI and SCI + Ad-control groups exhibited severe tissue damage, while the SCI + Ad-SIRT2 group showed less damage than the SCI group(Fig. 4A). Nissl staining indicated that after spinal cord injury, normal neurons appeared round and deeply stained, whereas damaged neurons were shrunken and light purple. Compared to the sham group, the SCI group had a reduced number of neurons. In contrast, the SCI + Ad-SIRT2 group had more neurons and improved neuronal morphology compared to the SCI + Ad-control group(Fig. 4B). These pathological results suggest that SIRT2 significantly inhibits tissue pathology and neuronal damage in SCI rats.

In motor function tests, we evaluated the impact of SIRT2 on motor recovery by measuring BBB scores on days 1, 3, 7, 14, 21, and 28 post-SCI. All rats had a BBB score of 21 before SCI, and immediately after SCI, the score dropped to 0, indicating acute lower limb paralysis. Over time, scores began to increase, but remained below those of the sham group in all SCI groups. In the first week post-SCI, there was little difference among the groups. By the second week, the SCI + Ad-SIRT2 group showed accelerated recovery; by day 28, the BBB scores of the SCI + Ad-SIRT2 group were significantly higher than those of the SCI and SCI + Ad-control groups, though still lower than the sham group, with statistically significant differences. The inclined plane test showed similar trends to the BBB test, indicating that overexpression of SIRT2 effectively promotes motor function recovery(Figure.4C)

(A): HE staining images of the spinal cord. Scale bar: 50 μm. (n = 10). (B): Nissl staining images of the spinal cord. Scale bar: 50 μm. (C): BBB scores and inclined plane test results at 1, 3, 7, 14, 21, and 28 days post-injury (N = 10; *P < 0.05, **P < 0.01, ***P < 0.001, ****P < 0.0001).

4 Discussion

Spinal cord injury (SCI) is a severe traumatic disease of the central nervous system that leads to the death of spinal neurons and the disruption of nerve fibers responsible for information transmission. This results in dysfunctions of sensory, motor, and autonomic nerves, with high rates of disability and mortality(21). Surgical intervention is the primary treatment; however, effective therapies for secondary cascade reactions are lacking(22). Stem cell transplantation has been considered a potential treatment, but it faces challenges such as low survival rates, tumorigenicity, and poor transplantation localization(23) .

Post-SCI, the affected area often experiences neuroinflammation, lipid peroxidation, oxidative stress, and ionic imbalances, including iron ions. These mechanisms can lead to various forms of programmed cell death, such as apoptosis, autophagy, cuproptosis, and ferroptosis. Iron ions are essential for normal neural functions, and iron overload has been positively correlated with SCI severity, possibly causing imbalances in ROS and the antioxidant system(24). Inhibiting neuronal ferroptosis can suppress the Fenton reaction, reduce ROS production, alleviate oxidative damage, and mitigate SCI.

Recent experiments have demonstrated that iron-dependent lipid peroxidation plays a critical role in several neurological diseases, including traumatic central nervous system injuries like SCI (25, 26). Neurons, with their phospholipid membranes rich in polyunsaturated fatty acid residues, have limited ROS scavenging capabilities, making them susceptible to oxidative stress. Ferroptosis is significantly involved in the progression of SCI (27).

We simulated ferroptosis in PC12 cells using Rsl3 and observed changes in ferroptosis-related factors, confirming the successful construction of the ferroptosis model (Figs. 1C and 2). In in vivo experiments, we modeled SCI in male rats and found significantly reduced GPX4 expression and elevated 4HNE levels in the spinal cords of these rats (Fig. 3C). These findings align with the known characteristics of ferroptosis, including increased Fe2+, lipid ROS accumulation, decreased GSH, and increased MDA (Figs. 1C, 3A). Therefore, ferroptosis indeed plays a role in the pathological process of SCI (8) .

SIRT2 is a NAD+-dependent deacetylase. It regulates metabolic pathways and various cellular functions, such as mitosis, cell differentiation, stress responses, cell survival, and homeostasis, through post-translational modifications of target genes, playing crucial roles in health and disease. Zylberberg B et al. found that resveratrol, by regulating SIRT2, inhibited excitotoxic damage in mouse spinal cords, providing neuroprotective effects (28). Feng YQ et al. reported that NAD precursors promoted spermatogenesis recovery in mice by inhibiting SIRT2-regulated ferroptosis(29). However, the relationship between SIRT2 and ferroptosis-induced SCI has not been studied.

In our study, we used recombinant adenovirus to overexpress SIRT2 in PC12 cells (Figs. 1A ,B). Comparisons among different groups revealed that SIRT2 significantly inhibited Rsl3-induced oxidative stress in PC12 cells (Fig. 1C). Staining of pathological tissue sections from rats showed that SIRT2 markedly inhibited tissue pathology and neuronal damage in SCI rats (Figs. 4A ,B). Similarly, the results from electron microscopy also demonstrated a comparable trend of changes (Figs. 3F). Moreover, motor function tests indicated that SIRT2 significantly promoted the recovery of motor function in SCI rats (Fig. 4C). Our study is the first to demonstrate both in vitro and in vivo that SIRT2 has the capacity to inhibit neuronal ferroptosis following SCI, thereby reducing SCI-induced damage.

Subsequently, we investigated the pathways through which SIRT2 influences ferroptosis.p53 is a crucial tumor suppressor gene that influences disease progression by regulating ferroptosis during tumor development.Tan Xinmin's team discovered that upregulating the p53 signaling pathway reduces lipid peroxidation-induced ferroptosis, ultimately inhibiting triple-negative breast cancer (30).p53 not only regulates ferroptosis in cancer mechanisms but also influences the occurrence and progression of

diseases in various systems by controlling ferroptosis.Qu Zhi's team found that p53 can interact with NAT10 to promote ferroptosis in cardiomyocytes, thereby exacerbating the positive feedback loop of cardiac I/R injury (31).In the nervous system, Mena Anla Yousuf et al. discovered that spermidine significantly reduces p53 protein levels and inhibits Alzheimer's disease in rats by regulating ferroptosis (32).These studies highlight the critical role of p53 in regulating cell metabolism and oxidative stress responses.Therefore, we verified the roles of SIRT2 and p53 in spinal cord neuron ferroptosis, consistent with previous research findings.Upregulation of SIRT2 significantly inhibits p53 expression, while upregulation of p53 significantly reverses the inhibitory effect of SIRT2 on ferroptosis (Fig. 3B).In cell experiments, we further confirmed this result by adding the p53 agonist Nutlin-3a to the SCI + Ad-SIRT2 group (Fig. 2A).Yan Mi et al. found that activating Nrf2 can inhibit ferroptosis by suppressing mitochondrial ROS production, thereby alleviating ischemic brain injury in rats (33).Chen Junhui's team also discovered that OA promotes the translocation of Nrf2 from the cytoplasm to the nucleus, thereby activating the Nrf2/GPX4 pathway and inhibiting neuronal ferroptosis, providing neuroprotection (34).These studies indicate that activation of Nrf2 can provide neuroprotection by inhibiting ferroptDenada Dibra's team revealed that mutant p53 protects cells from ferroptosis through Nrf2-dependent regulation of Mgst3 and Prdx6 (35).osis.Is there an upstream-downstream regulatory relationship between p53 and Nrf2 that influences ferroptosis?We also hypothesize that the expression of Nrf2 in neurons after SCI is regulated by both SIRT2 and p53.Our in vitro and in vivo experiments confirmed this hypothesis and are consistent with previous results.We found that in rats and PC12 cells, Nrf2 is indeed regulated by p53, and the effect of p53 on Nrf2 is reversed with the overexpression of SIRT2 (Fig. 2A).

Our research suggests that SIRT2 may inhibit post-SCI neuronal ferroptosis by regulating the expression of p53/Nrf2.In our cell and animal experiments, we verified the changes in p53 and Nrf2 expression levels through SIRT2 overexpression to determine their potential relationship and found that these changes affect the levels of ferroptosis-related genes and factors.For example, in our cell experiments, we found that oxidative stress-related factors ROS and MPO were significantly elevated, while SOD was significantly reduced in PC12 cells (Fig. 1C).In the spinal cord tissue of SCI rats, GSH levels were significantly reduced, while MDA and iron levels were significantly elevated (Fig. 3A).These results indicate that changes in the p53/Nrf2 pathway induced by SIRT2 overexpression affect ferroptosis.In cell and animal experiments, the gene and protein expression levels of ferroptosis-related genes GPX4 and ferroptosis-related markers 4HNE confirmed this hypothesis (Figs. 2B, 3C).The results of the above experiment were also confirmed by immunofluorescence analysis (Fig. 3E). Additionally, staining results of pathological tissue sections of rats indicated that SIRT2 significantly inhibits tissue lesions and neuronal damage in SCI rats (Figs. 4A, B).We monitored the motor functions of rats in different groups and found that SIRT2 effectively promotes the recovery of motor function.Based on experimental results, we infer that these effects are achieved by regulating the changes in the levels of the aforementioned genes.

5 Conclusion

SIRT2 is a potential therapeutic target for treating spinal cord injury (SCI).SIRT2 can reduce neuronal ferroptosis after SCI by regulating the p53/Nrf2 signaling pathway, thereby alleviating SCI and promoting motor function recovery in SCI rats.

Abbreviations

SCI
spinal cord injury
SIRT2
Sirtuin 2
GPX4
glutathione peroxidase 4
4HNE
4-hydroxynonenal
ROS
reactive oxygen species
SOD
superoxide dismutase
MPO
myeloperoxidase
BBB
Basso, Beattie, and Bresnahan
H&E
Hematoxylin and Eosin
GSH
glutathione
MDA
malondialdehyde
WB
western blot

Declarations

7 Ethics approval and Consent to Participate

This experimental protocol was approved by the Ethics Committee of the Affiliated Hospital of Zhongshan Hospital (Approval Number: DW2024-063-01).

8 Clinical Trial Number

Not applicable.

9 Data Availability Statement

The original contributions presented in the study are included in the article/Supplementary Materials, further inquiries can be directed to the corresponding authors.

10 Conflict of Interest

The authors declare that the research was conducted in the absence of any commercial or financial relationships that could be construed as a potential conflict of interest.

11 Funding

The authors disclose receipt of the following financial or material support for the research, authorship.and/or publication of this article: This study was supported by Dalian Science and Technology Innovation Fund (2021JJ13SN68) and Department of Education of Liaoning Province(LJ232411258003).

Author Contribution

ZZ , SS and HF conceived the idea for the study, led study design and data collection, conducted the statistical analyses, interpreted the data, and drafting of manuscript; YC,ZH, and ZW performed the experiments and analyzed data ZZ, WZ and WT revised the article for important intellectual content; ZY, ZM and GJ collected the data and helped in the statistical analyses. All authors read and approved the final manuscript and agreed on its submission.

13 Acknowledgments

Not applicable.

References

1. Zipser CM, Cragg JJ, Guest JD, Fehlings MG, Jutzeler CR, Anderson AJ, et al. Cell-based and stem-cell-based treatments for spinal cord injury: evidence from clinical trials. Lancet Neurol. 2022;21(7):659 – 70.

2. Zou Z, Liu R, Wang Y, Tan H, An G, Zhang B, et al. Protein arginine methyltransferase 8 regulates ferroptosis and macrophage polarization in spinal cord injury via glial cell-derived neurotrophic factor. CNS Neurosci Ther. 2023;29(8):2145-61.

3. Zhang X, Jiang W, Lu Y, Mao T, Gu Y, Ju D, et al. Exosomes combined with biomaterials in the treatment of spinal cord injury. Front Bioeng Biotechnol. 2023;11:1077825.

4. Corrigendum: Deferoxamine promotes recovery of traumatic spinal cord injury by inhibiting ferroptosis. Neural Regen Res. 2019;14(6):1068.

5. Bersuker K, Hendricks JM, Li Z, Magtanong L, Ford B, Tang PH, et al. The CoQ oxidoreductase FSP1 acts parallel to GPX4 to inhibit ferroptosis. Nature. 2019;575(7784):688 – 92.

6. Hirschhorn T, Stockwell BR. The development of the concept of ferroptosis. Free Radic Biol Med. 2019;133:130 – 43.

7. Xu J, Ding Y, Shi C, Yuan F, Sheng X, Liu Y, et al. Identification of Cathepsin B as a Therapeutic Target for Ferroptosis of Macrophage after Spinal Cord Injury. Aging Dis. 2023;15(1):421 – 43.

8. Kang Y, Zhu R, Li S, Qin KP, Tang H, Shan WS, et al. Erythropoietin inhibits ferroptosis and ameliorates neurological function after spinal cord injury. Neural Regen Res. 2023;18(4):881-8.

9. Chen Y, Liu S, Li J, Li Z, Quan J, Liu X, et al. The Latest View on the Mechanism of Ferroptosis and Its Research Progress in Spinal Cord Injury. Oxid Med Cell Longev. 2020;2020:6375938.

10. Chen M, Tan J, Jin Z, Jiang T, Wu J, Yu X. Research progress on Sirtuins (SIRTs) family modulators. Biomed Pharmacother. 2024;174:116481.

11. Li HW, Zhang HH. The Protein Acetylation after Traumatic Spinal Cord Injury: Mechanisms and Therapeutic Opportunities. Int J Med Sci. 2024;21(4):725 – 31.

12. Liu Y, Zhang Y, Zhu K, Chi S, Wang C, Xie A. Emerging Role of Sirtuin 2 in Parkinson's Disease. Front Aging Neurosci. 2019;11:372.

13. He M, Chiang HH, Luo H, Zheng Z, Qiao Q, Wang L, et al. An Acetylation Switch of the NLRP3 Inflammasome Regulates Aging-Associated Chronic Inflammation and Insulin Resistance. Cell Metab. 2020;31(3):580 – 91.e5.

14. Zhang X, Song T, Zhao M, Tao X, Zhang B, Sun C, et al. Sirtuin 2 Alleviates Chronic Neuropathic Pain by Suppressing Ferroptosis in Rats. Front Pharmacol. 2022;13:827016.

15. Chauhan S, Jaiswal S, Jakhmola V, Singh B, Bhattacharya S, Garg M, et al. Potential role of p53 deregulation in modulating immune responses in human malignancies: A paradigm to develop immunotherapy. Cancer Lett. 2024;588:216766.

16. Xu R, Wang W, Zhang W. Ferroptosis and the bidirectional regulatory factor p53. Cell Death Discov. 2023;9(1):197.

17. Agborbesong E, Zhou JX, Li LX, Harris PC, Calvet JP, Li X. Prdx5 regulates DNA damage response through autophagy-dependent Sirt2-p53 axis. Hum Mol Genet. 2023;32(4):567 – 79.

18. Zhao M, Zhang X, Tao X, Zhang B, Sun C, Wang P, et al. Sirt2 in the Spinal Cord Regulates Chronic Neuropathic Pain Through Nrf2-Mediated Oxidative Stress Pathway in Rats. Front Pharmacol. 2021;12:646477.

19. Zhang J, Hong Y, Cao W, Yin S, Shi H, Ying W. SIRT2, ERK and Nrf2 Mediate NAD(+) Treatment-Induced Increase in the Antioxidant Capacity of PC12 Cells Under Basal Conditions. Front Mol Neurosci. 2019;12:108.

20. Wu J, Han W, Zhang Y, Li S, Qin T, Huang Z, et al. Glutamine Mitigates Oxidative Stress-Induced Matrix Degradation, Ferroptosis, and Pyroptosis in Nucleus Pulposus Cells via Deubiquitinating and Stabilizing Nrf2. Antioxid Redox Signal. 2024;41(4–6):278 – 95.

21. Hutson TH, Di Giovanni S. The translational landscape in spinal cord injury: focus on neuroplasticity and regeneration. Nat Rev Neurol. 2019;15(12):732 – 45.

22. Zhu H, Guest JD, Dunlop S, Xie JX, Gao S, Luo Z, et al. Surgical intervention combined with weight-bearing walking training promotes recovery in patients with chronic spinal cord injury: a randomized controlled study. Neural Regen Res. 2024;19(12):2773-84.

23. Ju D, Dong C. The combined application of stem cells and three-dimensional bioprinting scaffolds for the repair of spinal cord injury. Neural Regen Res. 2024;19(8):1751-8.

24. Hellenbrand DJ, Quinn CM, Piper ZJ, Elder RT, Mishra RR, Marti TL, et al. The secondary injury cascade after spinal cord injury: an analysis of local cytokine/chemokine regulation. Neural Regen Res. 2024;19(6):1308-17.

25. Cui M, Chen F, Shao L, Wei C, Zhang W, Sun W, et al. Mesenchymal stem cells and ferroptosis: Clinical opportunities and challenges. Heliyon. 2024;10(3):e25251.

26. Li QS, Jia YJ. Ferroptosis: a critical player and potential therapeutic target in traumatic brain injury and spinal cord injury. Neural Regen Res. 2023;18(3):506 – 12.

27. Geng H, Li Z, Li Z, Zhang Y, Gao Z, Sun L, et al. Restoring neuronal iron homeostasis revitalizes neurogenesis after spinal cord injury. Proc Natl Acad Sci U S A. 2023;120(46):e2220300120.

28. Zylberberg B, Poodts M, Roncoroni J, Coronel MF, Mazzone GL. Resveratrol evokes neuroprotective effects and improves foot stance following kainate-induced excitotoxic damage to the mouse spinal cord. Neuropharmacology. 2024;250:109906.

29. Feng YQ, Liu X, Zuo N, Yu MB, Bian WM, Han BQ, et al. NAD(+) precursors promote the restoration of spermatogenesis in busulfan-treated mice through inhibiting Sirt2-regulated ferroptosis. Theranostics.

2024;14(6):2622-36.

30. Tan X, Kong D, Tao Z, Cheng F, Zhang B, Wang Z, et al. Simultaneous inhibition of FAK and ROS1 synergistically repressed triple-negative breast cancer by upregulating p53 signalling. Biomark Res. 2024;12(1):13.

31. Qu Z, Pang X, Mei Z, Li Y, Zhang Y, Huang C, et al. The positive feedback loop of the NAT10/Mybbp1a/p53 axis promotes cardiomyocyte ferroptosis to exacerbate cardiac I/R injury. Redox Biol. 2024;72:103145.

32. Youssef MAM, Mohamed TM, Bakry AA, El-Keiy MM. Synergistic effect of spermidine and ciprofloxacin against Alzheimer's disease in male rat via ferroptosis modulation. Int J Biol Macromol. 2024;263(Pt 2):130387.

33. Mi Y, Wang Y, Liu Y, Dang W, Xu L, Tan S, et al. Kellerin alleviates cerebral ischemic injury by inhibiting ferroptosis via targeting Akt-mediated transcriptional activation of Nrf2. Phytomedicine. 2024;128:155406.

34. Chen J, Shi Z, Zhang C, Xiong K, Zhao W, Wang Y. Oroxin A alleviates early brain injury after subarachnoid hemorrhage by regulating ferroptosis and neuroinflammation. J Neuroinflammation. 2024;21(1):116.

35. Dibra D, Xiong S, Moyer SM, El-Naggar AK, Qi Y, Su X, et al. Mutant p53 protects triple-negative breast adenocarcinomas from ferroptosis in vivo. Sci Adv. 2024;10(7):eadk1835.

Figures

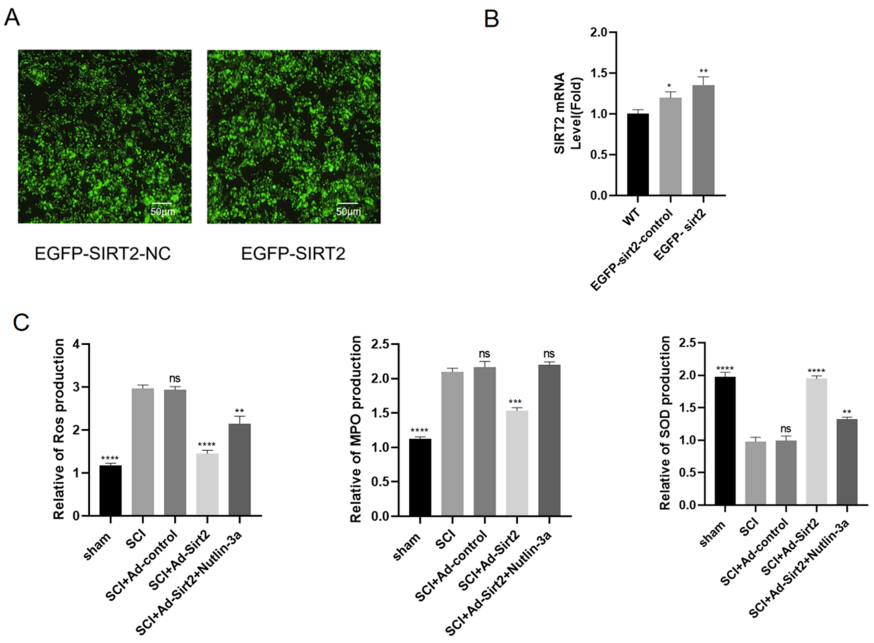


Figure 1

Overexpression of SIRT2 inhibits oxidative stress in PC12 cells.

(A):The fluorescence images of transfected PC12 cells in the SIRT1 intervention group and the blank vector control group, Scale bar : 50 μm.(B):qRT-PCR analysis of SIRT2 expression levels (C):Measurement of intracellular ROS, MPO, and SOD levels.□*P <0.05□**P□0.01□***P□0.001□****P□ 0.0001 vs.SCI group□***P□0.001 vs.0 μmol/L group□□

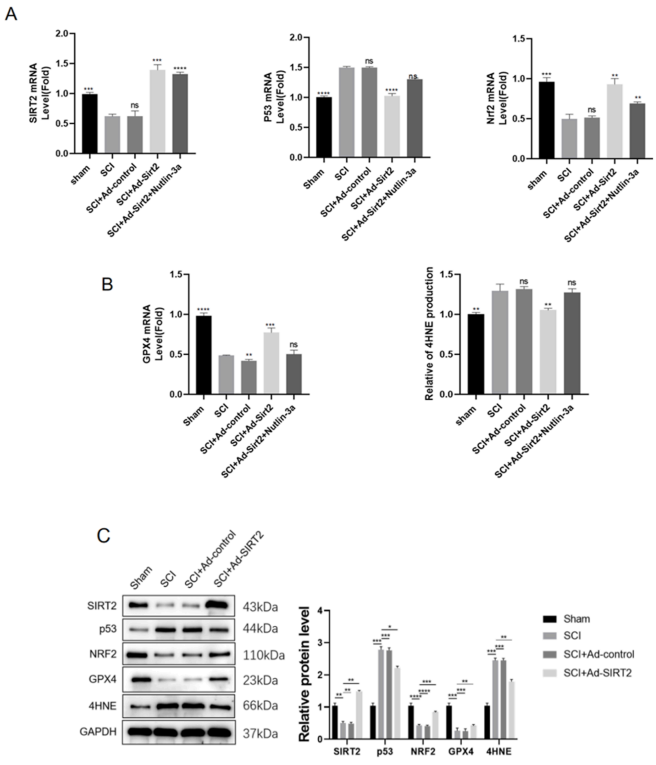


Figure 2

SIRT2 inhibits ferroptosis in PC12 cells by regulating p53 and Nrf2.

A: mRNA expression levels of SIRT2, p53, and Nrf2.B: mRNA expression levels of GPX4 and measurement of intracellular 4HNE level.C: Western blot bands for SIRT2, p53, Nrf2, GPX4, 4HNE, and GAPDH. (*P < 0.05, **P < 0.01, ***P < 0.001, ****P < 0.0001 vs. SCI group)

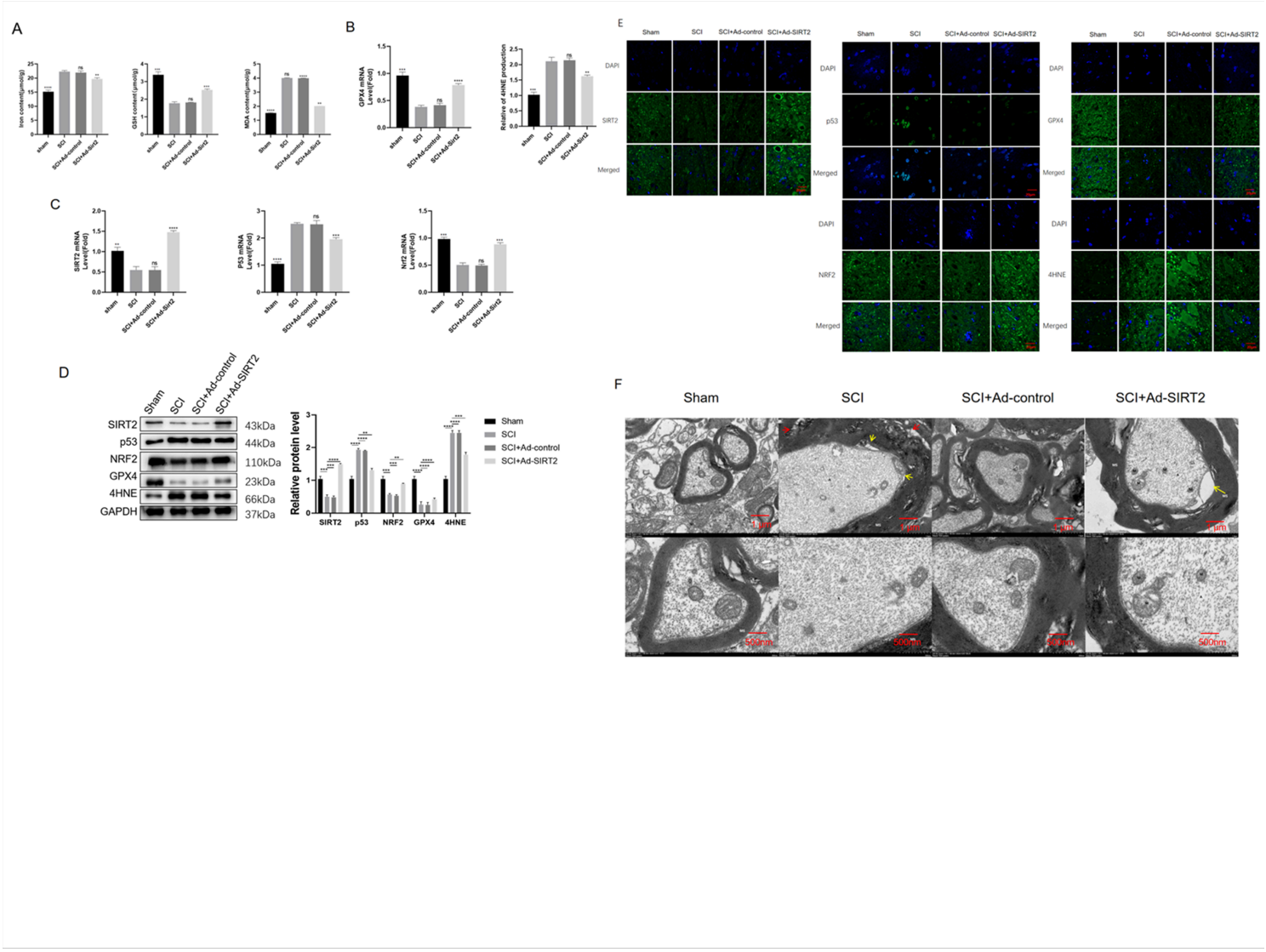


Figure 3

Injection of adenovirus overexpressing SIRT2 inhibits ferroptosis after SCI in rats.

A: Measurement of iron, GSH, and MDA levels in spinal cord tissues of each group.B: mRNA expression levels of SIRT2, p53, and Nrf2 in spinal cord tissues of each group.C: mRNA expression levels of GPX4 and measurement of 4HNE level in spinal cord tissues of each group.D: Western blot bands for SIRT2, p53, Nrf2, GPX4, 4HNE, and GAPDH in spinal cord tissues of each group (N=10; *P < 0.05, **P < 0.01, ***P < 0.001, ****P< 0.0001). E: Immunofluorescence study on the expression of SIRT2, P53, Nrf2, GPX4 and 4HNE in spinal cord tissue of rats with spinal cord injury. Fluorescence microscopy results of SIRT2, P53, Nrf2, GPX4 and 4HNE and DAPI. Green indicates SIRT2, P53, Nrf2, GPX4 and 4HNE in spinal cord tissue, and blue indicates nuclei stained by DAPI. Scale bar: 50 μm. F:Transmission electron microscopy images. The morphology of mitochondria differs between groups. Arrows show mitochondria of spinal cord neurons. Boxes show high magnification views of low magnification images. Scale bars: 1 μm (upper panels) and 500 nm (lower panels).

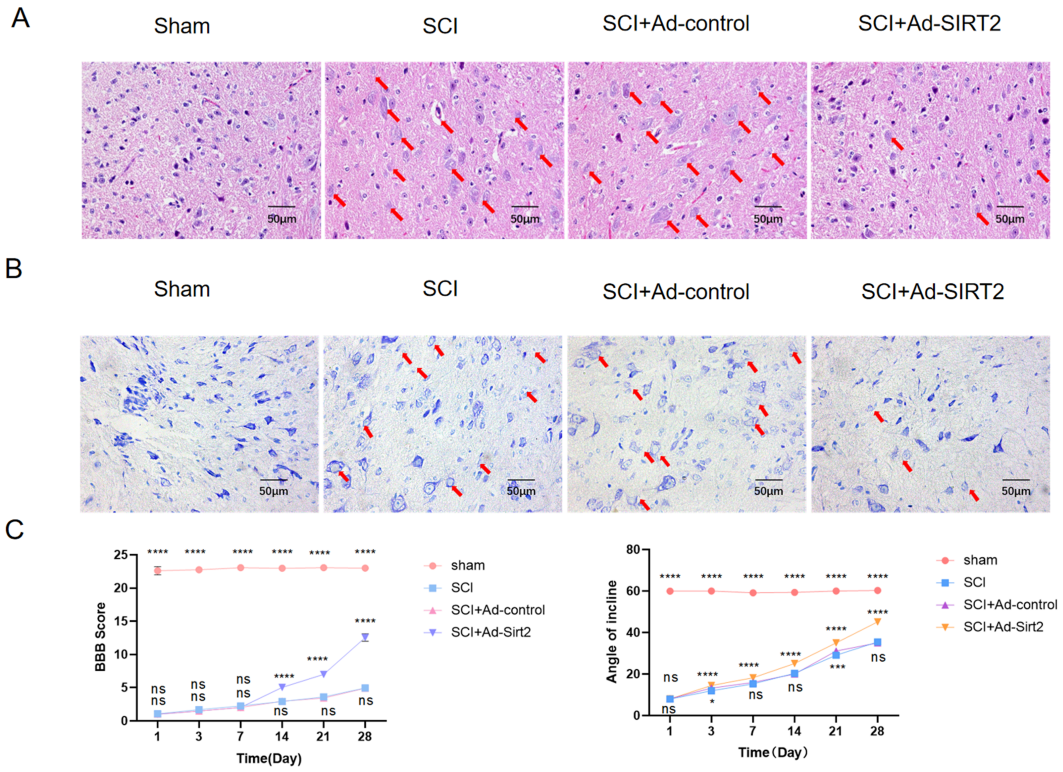


Figure 4

Overexpression of SIRT2 promotes neuronal repair and motor function recovery in SCI rats.

(A): HE staining images of the spinal cord. Scale bar: 50 μm. (n=10) . (B): Nissl staining images of the spinal cord. Scale bar: 50 μm. (C): BBB scores and inclined plane test results at 1, 3, 7, 14, 21, and 28 days post-injury (N=10; *P < 0.05, **P < 0.01, ***P < 0.001, ****P< 0.0001).

Supplementary Files

This is a list of supplementary files associated with this preprint. Click to download.

- Graphicalabstract.tif